RSC Advances

PAPER

View Article Online
View Journal | View Issue

Cite this: *RSC Adv.*, 2022, **12**, 11119

Real-time drug release monitoring from pH-responsive CuS-encapsulated metal–organic frameworks†

Bei Liu,[a] Lirong Sun,[a] Xijian Lu,[a] Yuping Yang,[a] Hongshang Peng,[a] Zhaogang Sun,*[b] Juan Xu*[c] and Hongqian Chu*[b]

Received 24th December 2021
Accepted 4th April 2022

DOI: 10.1039/d1ra09320g

rsc.li/rsc-advances

Real-time monitoring of drug release behaviors over extended periods of time is critical in understanding the dynamics of drug progression for personalized chemotherapeutic treatment. In this work, we report a metal–organic framework (MOF)-based nanotheranostic system encapsulated with photothermal agents (CuS) and therapeutic drug (DOX) to achieve the capabilities of real-time drug release monitoring and combined chemo-photothermal therapy. Meanwhile, folic acid-conjugated polyethylene glycol (FA-PEG) antennas were connected to the MOF through coordination interactions, endowing the MOF with an enhanced active targeting effect toward cancer cells. It is anticipated that such a theranostic agent, simultaneously possessing tumor-targeting, real-time drug monitoring and effective treatment, will potentially enhance the performance in cancer therapy.

Introduction

Over the past few decades, construction of "Smart" drug delivery systems (DDSs) with specific responsiveness to pH,[1,2] temperature,[3] light irradiation,[4,5] *etc.* has attracted great attention in the biomedical field.[6–8] This strategy provides a great opportunity to overcome the disadvantages of drug molecules, such as the poor solubility, low stability and excessive systemic toxicity. Despite exhaustive efforts, a formidable challenge of DDSs is the lack of general applicability for all patients owing to individual differences and variable physical fitness.[9] Under these circumstances, DDSs with real-time monitoring of drug release/activation are of significant importance for personalized cancer therapy.

So far, several DDSs with drug release monitoring have been developed.[10–19] These DDSs can provide opportunities to evaluate the therapeutic effectiveness, and export useful information for dose adjustment and prognosis for personalized medicine. For example, Zheng and co-workers[18] used carbon nanodots as both fluorophore and drug nanocarrier for real-time monitoring of drug release on the basis of the Förster resonance energy transfer (FRET) signal. Xing *et al.*[19] conjugated photoactivatable platinum(IV) prodrugs and caspase imaging peptides on the silica-coated upconversion-luminescent nanoparticles, achieving the real-time and *in situ* reporting of drug activation. Though effective, these approaches are often limited by the expensive, time-consuming and ineffective post-modification or conjugation steps. Design of a simple but effective strategy for synthesizing smart DDS with real-time monitoring of drug release is highly desirable.

Metal–organic frameworks (MOFs), constructed by self-assembly of organic linkers and metal or metal-oxo nodes, have showed a great promise in the field of gas storage/separations, catalysis and nanomedicine.[20–28] Especially, the tumor microenvironment (TME)-responsive MOFs, including hypoxia-sensitive Cu-MOF[20] and acidic pH-degradable zeolitic imidazolate framework-8 (ZIF-8),[21,22] have been attracting emerging research efforts as ideal drug carriers. These MOFs possess the capability of efficient drug encapsulation and excellent controllable release property under the given stimulation, thus leading to a remarkably enhanced drug-delivery efficiency and minimal cytotoxicity upon degradation. However, construction of the TME-responsive MOFs that can simultaneously achieve real-time monitoring of drug release remains a great challenge. Moreover, the low specific tumor recognition together with the complexed preparation protocol also limited the future medical usage and clinical translation of these TME-responsive MOFs.

Herein, a new kind of "Smart" DDS with real-time drug release monitoring was developed based on the acidic pH-degradable MOFs. These nanotheranostics, referred to as CuS/D@Z-FA, were fabricated by encapsulating functional guests of photothermal agents (CuS) and therapeutic drug (DOX) within a well-defined ZIF-8 host, followed by the surface modification of

[a]College of Science, Minzu University of China, Beijing, 100081, China
[b]Translational Medicine Center, Beijing Chest Hospital, Capital Medical University/Beijing Tuberculosis and Thoracic Tumor Research Institute, Beijing, 101149, China. E-mail: sunzhaogang@bjxkyy.cn; chuhongqian@bjxkyy.cn
[c]National Research Institute for Family Planning, Beijing, 100005, China. E-mail: xujuan@nrifp.org.cn

† Electronic supplementary information (ESI) available. See https://doi.org/10.1039/d1ra09320g

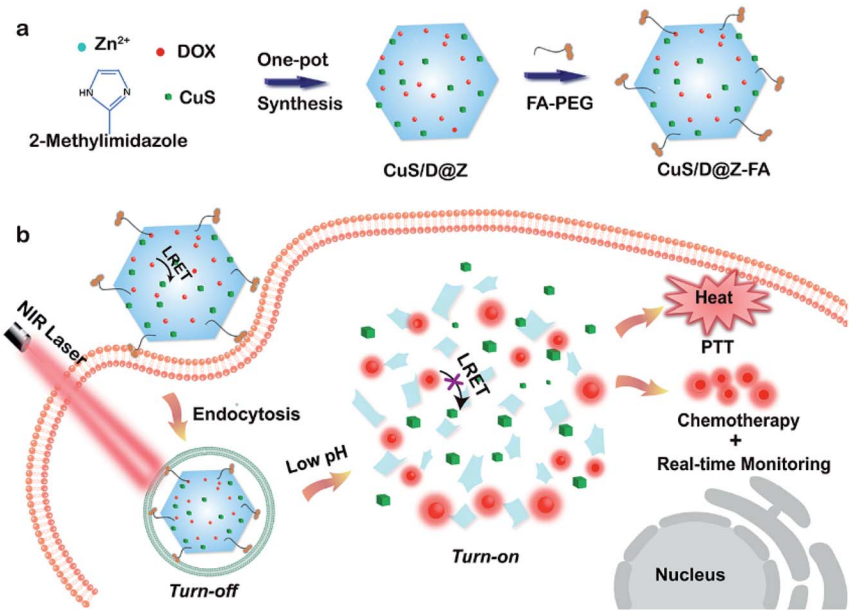

Scheme 1 (a) Schematic showing the synthesis process of CuS/D@Z-FA nanoparticles. (b) Schematic illustration of CuS/D@Z-FA for cancer treatment through a combination of NIR light-triggered PTT and pH-responsive drug release with real-time monitoring.

folic acid-conjugated polyethylene glycol (FA-PEG) antennas (Scheme 1). Upon the active accumulation of CuS/D@Z-FA in tumor cells through FA-receptor-mediated endocytosis, the coordination between zinc and imidazolate ions of ZIF-8 dissociated, resulting in the on-demand release of CuS and DOX for combined photothermal therapy (PTT) and chemotherapy (CT). Additionally, the FRET-quenched fluorescence of DOX in the nanoparticles can be gradually recovered upon the dissociation of ZIF-8, enabling the real-time drug release monitoring. These results highlight that this MOF-based nanoplatform is promising for high-performance cancer therapy.

Results and discussion

ZIF-8, a well-known subfamily of MOFs composed of Zn^{2+} ions and 2-methylimidazolate linkers, was chosen as the effective nanocarrier for anticancer drugs due to its good biocompatibility, desirable pH-sensitivity and exceptional encapsulation of different molecules/nanoparticles. Nanoscale ZIF-8 MOFs with a uniform size of 209 nm were firstly synthesized (Fig. S1†) through a reported bottom-up approach,[29] proving the synthesis feasibility of ZIF-8. Then multifunctional CuS/DOX@ZIF-8 (CuS/D@Z) nanoparticles were synthesized by efficiently encapsulating DOX and CuS into ZIF-8 during the one-pot assembly process. Briefly, methanol solutions of $Zn(NO_3)_2$ (12.5 mM) and 2-methyl imidazole (25 mM) were mixed at ambient conditions in the presence of DOX and pre-prepared CuS (~12.9 nm, Fig. 1a). After a quick vortex, the reaction solution was allowed to stand at room temperature for 24 hours. The products were collected by centrifugation, and washed several times with methanol. Fig. 1b presents the representative TEM image of the as-synthesized CuS/D@Z (217 nm, Fig. 1c) without any further purification. Small CuS nanoparticles can be clearly identified as the appearance of CuS has higher contrast compared with ZIF-8.

Notably, the synthesis approach allows to encapsulate CuS and DOX in an ultra-efficient and precisely controllable manner (Fig. 1d–f). CuS/D@Z NP in Fig. 1e were chosen for the following experiments, which can not only retain the hexagon shape and size uniformity of ZIF-8, but also possess reasonable amounts of CuS (59.375%, w/w) and DOX (2.083%, w/w) for further combined CT-PTT therapy. UV-vis-NIR absorption measurement (Fig. 1g, and S2†) confirms the successful encapsulation of CuS and DOX in CuS/D@Z owning to the existence of characteristic peaks of DOX centered at ~560 nm and a broad absorbance by CuS NPs (700–1100 nm). Note that the absorption spectrum of CuS/D@Z showed a remarkable broadening and redshift of DOX or CuS characteristic absorbance, mainly owing to the self-aggregate of DOX or CuS during the nanoparticle formation.

In order to prolong the blood circulation time and enhance the active tumor-targeting effect of nanoparticles, FA-PEG antennas were further functionalized on the surface of CuS/D@Z through coordination interaction of its carboxy groups with coordinatively unsaturated metal sites of Zn^{2+} on the surface of ZIF-8.[30,31] As shown in Fig. S3,† the resulting CuS/D@Z-FA NPs remained monodisperse in size without obvious shape change and aggregation. Zeta potential analysis (Fig. 1h) showed that CuS/D@Z were positively charged (+24.5 mV), and became negatively charged (−21.1 mV) after the attachment of FA-PEG. Additionally, the absorption peak at ~300 nm was the characteristic peak of FA, further confirming the successful functionalization of FA on the surface of CuS/D@Z (Fig. 1i).

The UV-vis-NIR absorption spectra of CuS/D@Z-FA showed a high absorbance in the NIR range (800–1100 nm), and the absorption intensity increased steadily with the increasing

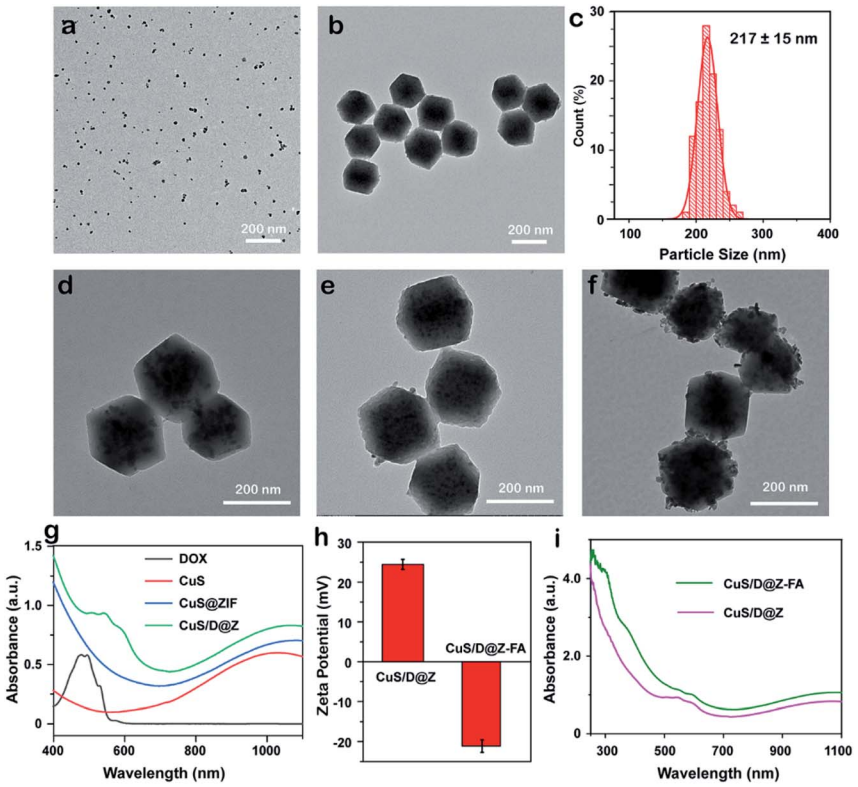

Fig. 1 TEM images of (a) CuS and (b) CuS/D@Z. (c) The corresponding size distribution of CuS/D@Z in (b). (d–f) TEM images of CuS/D@Z with different added amounts of DOX and CuS in the synthesis. (g) Absorption spectrum of DOX, CuS, CuS@ZIF and CuS/D@Z. (h) Zeta potential and (i) Absorption spectrum of CuS/D@Z and CuS/D@Z-FA.

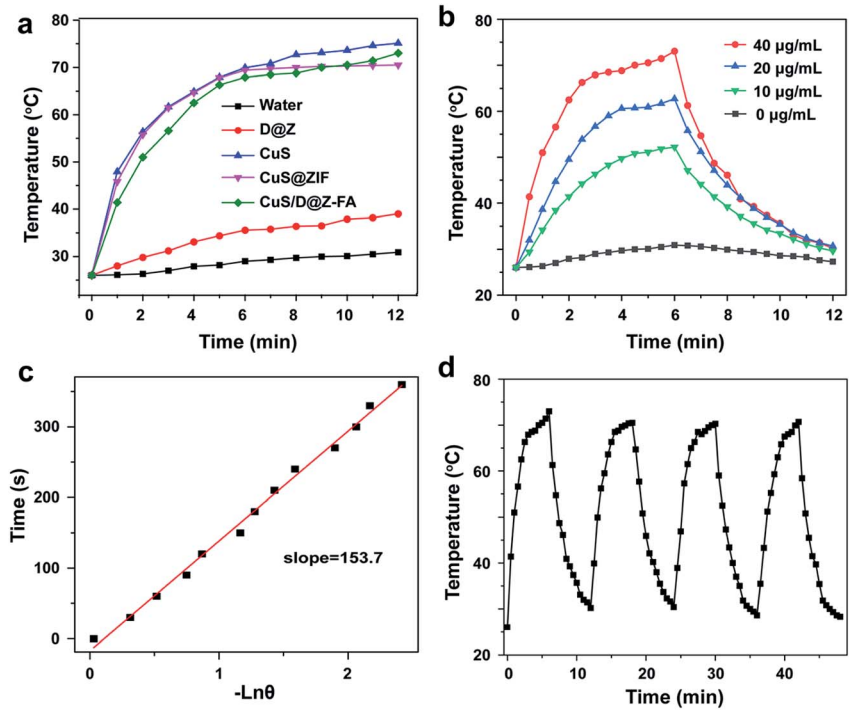

Fig. 2 (a) Irradiation time-dependent temperature changes of CuS, CuS@ZIF and CuS/D@Z-FA upon 808 nm irradiation. The laser was turned off after irradiation for 6 min. (b) Temperature variation curves for the aqueous dispersions containing different concentrations of CuS/D@Z-FA. (c) Plot of cooling time *versus* negative natural logarithm of the temperature driving force, obtained from the cooling stage as shown in (b). (d) Temperature changes of CuS/D@Z-FA over four ON/OFF irradiation cycles.

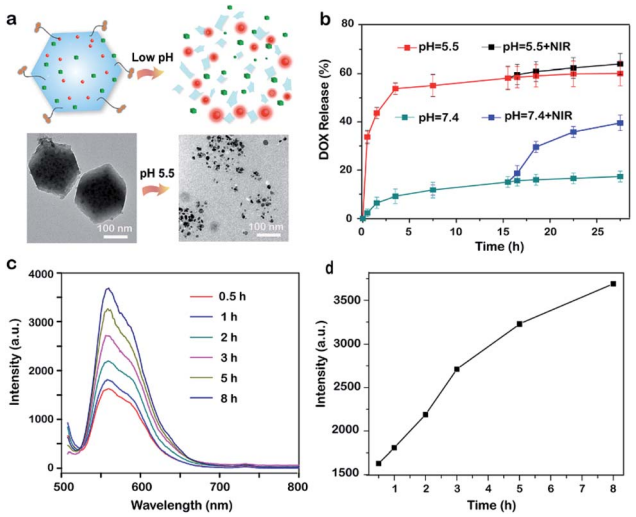

Fig. 3 (a) Schematic illustration and TEM images showing the pH-responsive decomposition of CuS/D@Z-FA. (b) DOX release profiles of CuS/D@Z-FA in PBS at pH 7.4 and 5.5 with/without 808 nm NIR irradiation. (c) Time-dependent emission spectra of DOX after immersing the NPs in PBS solution (pH 5.5). (d) Fluorescence intensity quantification of DOX obtained from (c).

concentrations of CuS/D@Z-FA (Fig. S4†). The significant absorption of CuS/D@Z-FA in the NIR window motivated us to investigate their photothermal properties. As shown in Fig. 2a, the temperature of CuS/D@Z-FA solution (40 μg mL^{-1}) increased rapidly with increased exposure time to the 808 nm NIR laser (1.0 W cm^{-2}), indicating that the NIR light harvesting by the CuS/D@Z-FA enabled effective heat generation. As a control, DI water or DOX@ZIF-8-FA (labeled as D@Z-FA) presented no significant increase of temperature under the same irradiation conditions. Moreover, CuS, CuS/D@Z and CuS/D@Z-FA NPs presented similar temperature profiles (Fig. 2a), suggesting the negligible impact of the ZIF-8 coating, DOX loading or FA-PEG modification on the photothermal effect of CuS.

The temperature variation curves of different concentrations of CuS/D@Z-FA were also conducted under the same 808 nm irradiation (1.0 W cm^{-2}). As expected, the temperature increase of CuS/D@Z-FA presented a concentration-dependent photothermal behavior (Fig. 2b). The photothermal conversion efficiency (η) of CuS/D@Z-FA was calculated as 38.11% according to the as-obtained data (Fig. 2b and c), which is comparable to that in previous reports.[32] Then the photothermal stability of CuS/D@Z-FA NPs was investigated by exerting four cycles of 808 nm NIR laser irradiation on CuS/D@Z-FA aqueous solution. As shown in Fig. 2d, CuS/D@Z-FA NPs remained a robust photothermal property. Therefore, the as-synthesized CuS/D@Z-FA NPs hold a great potential as promising candidates for PTT.

Since the coordination interaction between Zn^{2+} and 2-methylimidazolate ligand dissociates at pH 5.0–6.0 owing to the protonation effect, ZIF-8 NPs can degrade in acidic lysosomes of tumor cells (pH ~ 5.5, Fig. 3a), while stay stable under normal physiological conditions (pH ~ 7.4). Based on this line, pH-responsive release of DOX from CuS/D@Z-FA NPs were explored by immersing CuS/D@Z-FA NPs in PBS solutions with different pH values (pH 7.4 and 5.5). As illustrated in Fig. 3b, the DOX release profiles of CuS/D@Z-FA were obviously pH-dependent: the cumulative release amount of DOX could reach 60.1% at pH 5.5, which is much higher than that at pH 7.4 (17.3%). Considering that the tumor microenvironment of many solid tumors is mildly acidic, such pH-sensitive drug release property of CuS/D@Z-FA does great benefit for tumor-specific therapy. To be specific, the accumulated release ratio at pH 5.5 condition increased from 60.1 to 64.0% with the 808 nm laser irradiation, and a similar variation tendency was found at pH 7.4. Such enhancement of drug release mainly attributed to the increasing temperature generated by the CuS, which can accelerate the dissociation of CuS/D@Z-FA to release DOX. These results suggested that the as-synthesized CuS/D@Z-FA NPs had a pH-responsive and NIR-induced drug release behavior, which do a great benefit to enhance the cytotoxicity toward tumor cells selectively.

Interestingly, when CuS and DOX simultaneously encapsulated in ZIF-8 host, FRET occurred between DOX and CuS due to the close proximity of the two, leading to a low fluorescence signal background. To prove it, the fluorescence signal of DOX in both D@Z-FA and CuS/D@Z-FA were tested. Fig. S5† showed a strong depression of DOX fluoresce after co-encapsulation of CuS and DOX in ZIF-8 host, suggesting an efficient energy transfer process has occurred from the DOX to the CuS. Upon accumulation of CuS/D@Z-FA in the acidic environment (*e.g.*, pH = 5.5), the coordination between zinc and imidazolate ions of ZIF-8 dissociated, leading to the on-demand release of CuS and DOX to eliminate LRET. As a result, the fluorescence signal of DOX enhanced simultaneously (Fig. 3c and d), demonstrating the great potential of this nanoconstruct to monitor the drug release in real-time.

Then we verified the real-time monitoring capability of CuS/D@Z-FA *via* live-cell confocal laser scanning microscopy (CLSM). MCF-7 cells were incubated with CuS/D@Z-FA for 0.5 h, washed with PBS, and further cultured at 37 °C under 5% CO_2 for 1 h and 3 h. As presented in Fig. 4a and b, a negligible DOX fluorescence can be detected after 0.5 h incubation, indicating a limited DOX was released from CuS/D@Z-FA after 0.5 h incubation. With the extension of the culture time, the fluorescence intensity of DOX increased gradually due to the decreased FRET effect from DOX to CuS in living MCF-7 cells. Such time-dependent increasement of DOX fluorescence help to track the release behavior of drug, which plays an important role in avoiding insufficient or excess drug dosing for cancer therapy.

The specific cancer cell recognition and cellular uptake of NPs is an important but formidable challenge for drug delivery systems. Herein, we introduced PEG to enhance the biostability of NPs,[21] and decorated FA at the end of PEG chain as a targeted recognition for cancer cells. To prove it, the intracellular uptake efficiency of DOX@Z and DOX@Z-FA to MCF-7 cells was demonstrated by CLSM. Note that DOX@Z and DOX@Z-FA were chosen for the experiments in order to exclude the FRET effect from DOX to CuS. As shown in Fig. 5a, for DOX@Z-FA treated group, the cells exhibited more red-fluorescence signal of DOX

than those incubated with DOX@Z. Additionally, flow cytometry analysis (Fig. 5b and c) showed that the fluorescence intensity of cells treated with DOX@Z-FA was 3.1-fold higher than those treated with DOX@Z, indicating the enhanced cellular uptake of DOX@Z-FA NPs *via* FA-receptor-mediated endocytosis.

The *in vitro* cytotoxicity of the nanosystem against MCF-7 cells was then evaluated by CCK-8 assay. As presented in Fig. 6a, treatment with the only NIR light irradiation, CuS@ZIF or CuS@ZIF-FA did not decrease the cell viability significantly, demonstrating the negligible toxicity of the light irradiation or these NPs to MCF-7 cells. The cells treated with CuS@ZIF + NIR or CuS/D@Z showed a significant cytotoxicity compared with the control groups, confirming their PTT or CT effect as anti-tumor agents. Notably, photo-irradiated CuS@Z-FA showed higher cytotoxicity (59.0%) compared to that of the cells treated with CuS@Z + NIR (39.2%), indicating an enhanced potency could be achieved through the folic acid targeting effect. As expected, incubation of the cells with CuS/D@Z-FA followed by light irradiation led to a highest cell cytotoxicity (82.5%) due to the combinational effects of FA receptor-mediated targeting, PTT and CT. Similar results can also be observed by the calcein AM/propidium iodide (PI) assay. As shown in Fig. 6b, the calcein AM/PI staining results demonstrated that the MCF-7 cells treated with CuS/D@Z-FA show apparent fluorescence change from green to red color when compared with the control groups, implying the efficient killing effect of CuS/D@Z-FA on MCF-7 cells.

Inspired by the good performance of the nanoconstruct *in vitro*, we further explored the *in vivo* activity of CuS/D@Z-FA. Firstly, the metabolic kinetics of NPs were investigated. Cy5 labeled CuS/D@Z and CuS/D@Z-FA were administrated to MCF-7 tumor-bearing mice through the tail vein. *Ex vivo* fluorescence imagings of various harvested organs and tumors upon necropsy at different time points after injection were measured using *in vivo* imaging system (IVIS). As shown in Fig. S6,† the fluorescent intensity increased gradually and reached highest at 6 h postinjection, which may attribute to the degradation of ZIF-8 and the sustained release of Cy5 over time. Then the fluorescent intensity decreased, indicating the gradually clearance

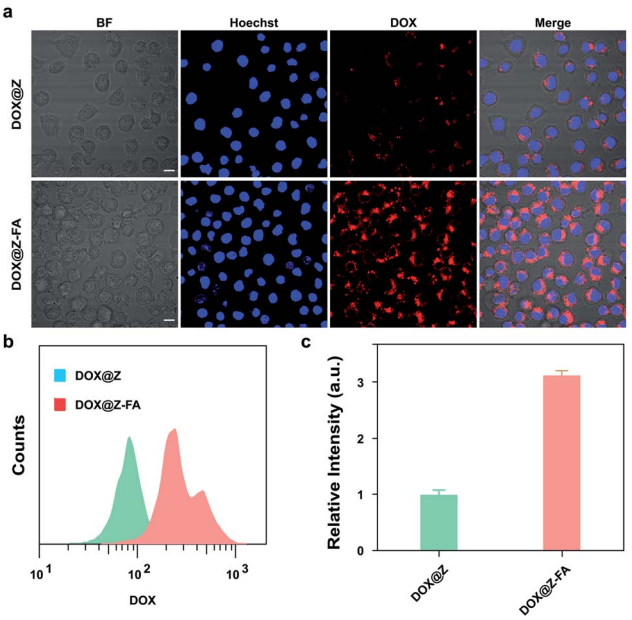

Fig. 5 (a) Confocal fluorescence images of MCF-7 cells. The cells were incubated with DOX@ZIF or DOX@ZIF-FA for 3 h. The cell nuclei were stained with Hoechst 33342. Scale bar: 20 μm. (b) Flow cytometric quantification of the cellular uptake of DOX@ZIF or DOX@ZIF-FA.

of NPs out of the body. Remarkably, CuS/D@Z-FA treated mice showed a much higher fluorescence intensity than CuS/D@Z-treated mice, demonstrating the satisfactory targeting ability of folic acid.

Then *in vivo* therapeutic efficacy of CuS/D@Z-FA NPs was evaluated. MCF-7 tumor-bearing mice were randomly divided into 5 groups (5 mice per group), treated with PBS, CuS@Z-FA, CuS@Z-FA + NIR, CuS/D@Z-FA, CuS/D@Z-FA + NIR, respectively. As presented in Fig. 7a, fast tumor growth was observed in the PBS or CuS@Z-FA groups. Treatment with CuS@Z-FA + NIR or CuS/D@Z-FA had moderate antitumor capability because of the PTT or CT. Notably, a strongest anti-tumor effect

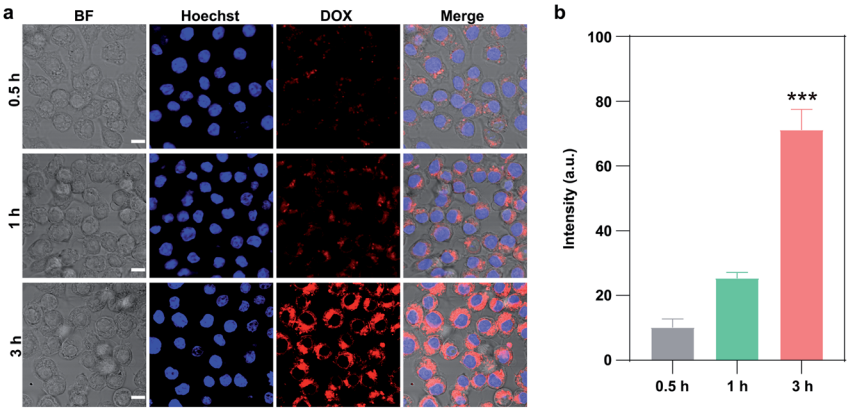

Fig. 4 (a) Confocal fluorescence images of MCF-7 cells. The cells were incubated with CuS/D@Z-FA for 0.5 h, subsequently washed with PBS, and further incubated for 1 h and 3 h with fresh culture medium. The cell nuclei were stained with Hoechst. Scale bar: 10 μm. (b) Quantitative analysis of DOX fluorescence in the cells at 0.5, 1, 2 and 3 h after incubation with CuS/D@Z-FA.

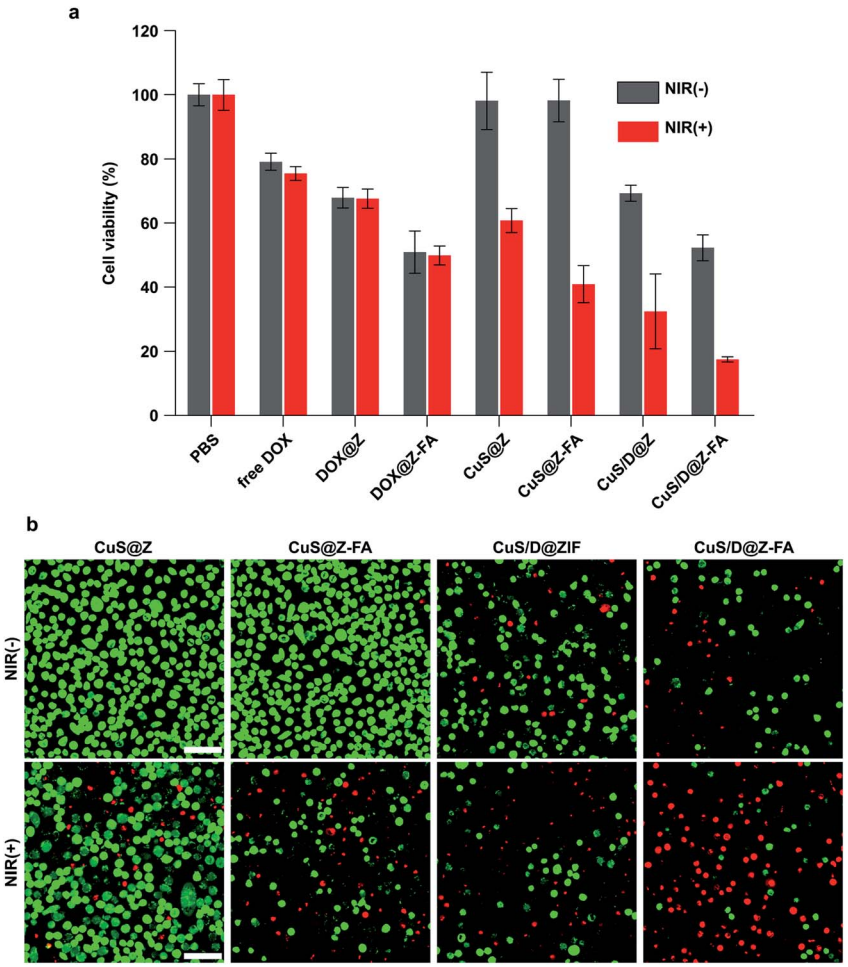

Fig. 6 (a) Viability of MCF-7 cells after different treatments. (b) Confocal fluorescence images of cell apoptosis by staining with Annexin V-FITC and PI after different treatments. Scale bar: 50 μm.

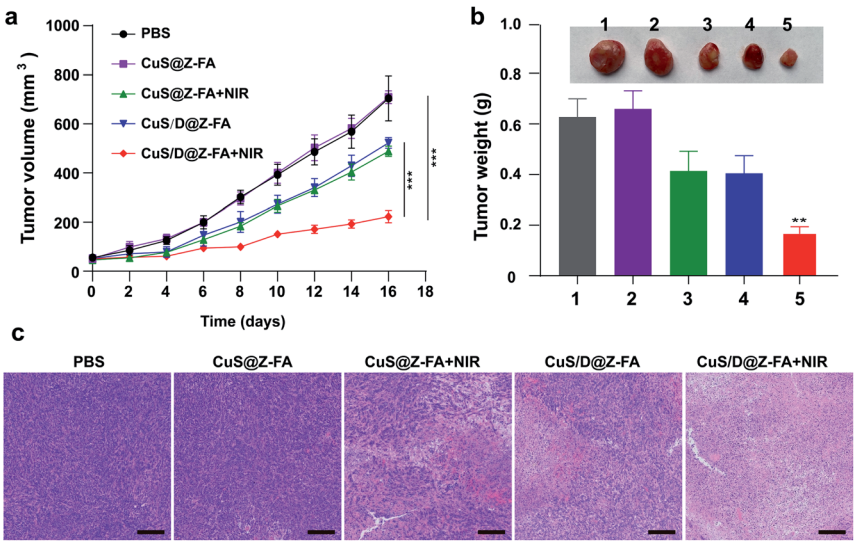

Fig. 7 (a) Tumor growth curves after different treatments. The data are presented as the mean ± SD ($n = 5$). $^{**}P < 0.01$, $^{***}P < 0.001$ (one-way ANOVA). (b) Representative images of the tumors excised from mice of the different treatment groups and tumor weights of mice at day 16 in the different treatment groups on dat 16 (1, PBS; 2, CuS@Z-FA; 3, CuS@Z-FA + NIR; 4, CuS/D@Z-FA; 5, CuS/D@Z-FA + NIR). $^{**}P < 0.01$ (one-way ANOVA). (c) H&E staining of tumor tissues from mice in the different treatment groups. Scale bars, 100 μm.

was achieved in the CuS/D@Z-FA + NIR group, implying that the combination of PTT and CT was more effective than either modality alone. Moreover, the final tumors of each group were dissected, and the weights and size of excised tumors were presented in Fig. 7b. As expected, mice treated with CuS/D@Z-FA + NIR showed a smaller tumor size compared with the other groups. The hematoxylin and eosin (H&E) stained sections of tumors were also shown in Fig. 7c. The results demonstrated the PTT/CT combined therapy can lead to a higher level of nucleus dissociation and necrosis than other groups.

The toxicity of CuS/D@Z-FA was further evaluated *in vivo*. As presented in Fig. S7,† the body weights of mice in all groups are increased steadily with time, implying little adverse side effect of NPs. Then the morphology of sectioned organs from mice after different treatments was studied. Fig. S8† showed that the main organs (kidney, heart, lung, liver and spleen) experienced no obvious changes in cellular integrity and tissue morphology, indicating the negligible systematic toxicity of CuS/D@Z-FA NPs. The results of serum biochemistry (Fig. S9†) also show that no significant changes of serum parameters occurred between the control group and the treatment groups, including the liver function markers of alanine aminotransferase (ALT) and aspartate aminotransferase (AST), the kidney function indicators of blood urea nitrogen (BUN) and creatinine (CRE).

Conclusions

In summary, we have developed a pH-responsive MOF-based nanotheranostic system by encapsulating photothermal agents (CuS) and therapeutic drug (DOX) into ZIF-8, followed by the surface modification with FA-PEG to locate NPs through an active tumor-targeting effect. The as-synthesized NPs showed acid pH-responsive degradation in a tumor microenvironment, resulting in a quick release of DOX and CuS for combined CT-PTT therapy. Notably, real-time imaging of drug release can be achieved to monitor the progression and assess the effectiveness of the chemotherapeutic treatment. The results indicated that such theranostic agent had good biocompatibility, effective tumor-cell internalization, real-time drug release monitoring and synergistic CT-PTT treatment of tumors.

Experimental

Materials

Cupric chloride ($CuCl_2 \cdot 2H_2O$), sodium sulfide ($Na_2S \cdot 9H_2O$) and methanol (99.5%) were bought from Aladdin. Doxorubicin hydrochloride (DOX) was purchased from TCI. $Zn(NO_3)_2 \cdot 6H_2O$ and 2-methyl imidazole were purchased from Sigma-Aldrich. *N*,*N*-Dimethylformamide (DMF, ≥99%) was bought from J&K. PEG-FA (molecular weight = 2000 Da) was provided by Shanghai Ponsure Biotech. Cy5 was purchased form Fanbo Biochemicals. Deionized water (Millipore Milli-Q grade) with resistivity of 18.2 MΩ was used in the experiments. Hoechst 33342 was acquired from Solarbio. PBS, DMEM medium and Annexin V Apoptosis Kit were bought from Sangon Biotech. Cell counting kit-8 (CCK-8) was purchased from Transgene Biotech. All chemicals were used as received without any further purification.

Instrumentations

Transmission electron microscopy (TEM) images of NPs were taken on the JEM-1200EX transmission electron microscope (JEOL, Japan). Scanning electron microscopy (SEM) images were taken on the SU8220 scan electron microscope (Hitachi Co. Ltd, Japan). UV/Vis and fluorescent spectra were recorded on a JASCO V-750 spectrophotometer and Hitachi F-4600 spectrometer, respectively. *In vitro* cytotoxicity assay was carried out on a ELx800 t microplate reader (BioTek, America). The confocal laser scanning microscopy (CLSM) images were conducted by using Olympus FluoView FV1000 confocal microscope (Olympus Corporation, Shinjuku, Tokyo, Japan).

Synthesis of CuS/D@Z-FA

PVP-modified CuS nanoparticles were firstly synthesized as following: 10 mL of $CuCl_2 \cdot 2H_2O$ (3.5 mg mL^{-1}) and 10 mL of PVP (20 mg mL^{-1}) were dissolved in 90 mL deionized water. After stirring for 30 min at room temperature, 0.8 mL of $Na_2S \cdot 9H_2O$ (60.5 mg mL^{-1}) was added into the above reaction system. Then the mixed solution was put into an oil bath kettle at 90 °C, keep stirring until a dark-green solution was obtained. After cooling to room temperature, the PVP-modified CuS NPs were collected by centrifugation, washed with methanol, and redispersed in 5 mL of methanol for future use.

2-Methyl imidazole methanol solution (6 mL, 8 mg mL^{-1}), CuS solution (3 mL) and DOX (2 mL, 1 mg mL^{-1}) were mixed with at room temperature, followed by the addition of 14 mL of Zn $(NO_3)_2 \cdot 6H_2O$ methanol solution. After a quick vortex, the well-mixed solution was allowed to stand at room temperature for 24 hours. The as-obtained CuS/D@Z NPs were collected by centrifugation, washed with DMSO for three times and re-dispersed in DMSO for future use. CuS@Z NPs were synthesized under the same reaction conditions but without adding DOX solution.

The CuS/D@Z-FA NPs were prepared by the functionalization with PEG-FA on the surface of CuS/D@Z through the formation of coordination bonds with Zn^{2+}. Briefly, CuS/D@Z NPs were dispersed in PEG-FA solution and then stirred for 48 h under room temperature. Then the final CuS/D@Z-FA NPs were obtained by centrifugation, washed three times with DMSO to completely wash off the free PEG-FA.

Drug release from CuS/D@Z-FA

The pH-responsive release profiles of DOX from CuS/D@Z-FA NPs were studied according to our previous report. Briefly, CuS/D@Z-FA NPs were collected by centrifugation and re-dispersed in 2 mL of pH = 7.4 and 5.5 phosphoric buffer solutions (PBS) under magnetic stirring. At the given time periods, the release media were collected by centrifugation and replaced by the same volume of fresh media. The release of DOX was measured by a UV-vis spectrophotometer.

Photothermal properties of CuS/D@Z-FA

To investigate the photothermal effect of CuS/D@Z-FA, aqueous suspensions of CuS/D@Z-FA with different concentrations (0, 10, 20 and 40 μg mL^{-1}) were prepared and irradiated with an 808 nm NIR laser (1.0 W cm^{-2}). The temperature of CuS/D@Z-FA solution was recorded using a thermal imaging camera (TiS65, Fluke, USA) every 30 s until the solution reached a steady-state temperature (6 min). The temperature of distilled water was used as control. To test the photothermal conversion efficiency, CuS/D@Z-FA aqueous solution was irradiated with 808 nm light for 6 min and then the laser was shut off. The time constant for heat transfer of CuS/D@Z-FA was calculated by applying linear time data *versus* ln θ from the cooling stage.

Cellular uptake assay

DMEM medium containing 10% FBS, 100 units per ml aqueous penicillin G and 100 μg mL^{-1} streptomycin was prepared for the cell culture. Human breast cancer cells (MCF-7) were seeded in a glass bottom dish (35 mm) and cultured at 37 °C in a humidified atmosphere containing 21% O_2 and 5% CO_2 for 24 h. Then fresh medium containing CuS/D@Z or CuS/D@Z-FA was added. After 1 h incubation, the cells were washed thoroughly with PBS three times to remove the uninternalized NPs. The cells were stained with Hoechst 33342, and imaged by Olympus FluoView FV1000 confocal microscope. During the imaging process, the pinhole and gain setting of the CLSM were kept constant.

CCK-8 assay

MCF-7 cells were seeded in 96-well microplates (8×10^3 cells per well) and cultured overnight. Fresh medium containing CuS@Z, CuS@Z-FA, CuS/D@Z and CuS/D@Z-FA was added and incubated for 4 h. Then the cells were washed with PBS and irradiated with 808 nm NIR light for 10 min (1.0 W cm^{-2}). After irradiation and another 24 h incubation, 100 μL fresh culture medium containing 10% CCK-8 was immediately added to each well for 2 h. Absorbance at 450 nm was measured using a microplate reader.

Cell apoptosis assessment

MCF-7 cells were seeded in 35 mm confocal dishes (NEST Biotechnology) at a density of 4×10^5 cells per well for 24 h. DMEM containing CuS@Z, CuS@Z-FA, CuS/D@Z and CuS/D@Z-FA was added and incubated for 4 h. Then the cells were washed with PBS, cultured with fresh medium, and irradiated with 808 nm NIR light for 10 min (1.0 W cm^{-2}). After 24 h incubation, cells were stained with calcein AM/PI double-stain kit (Abcam) according to the manufacturer's instructions.

In vivo imaging

All animal studies were performed in accordance with NIH guidelines, with the protocol approved by the Institutional Animal Care and Use Committee of Beijing Tuberculosis and Thoracic Tumor Research Institute. The female BALB/c mice (16–18 g) obtained from Vital River Animal Laboratories (Beijing, China) and maintained in a sterile environment. Xenograft tumor models were established by inoculating 4T1 cells (1×10^6 cells per 100 μL in 1 : 1 (v/v) PBS and Matrigel, BD bioscience) into the left flank of the mice. When the tumors reach to 200–400 mm^3, the mice were randomly divided into 2 groups for the treatment with CuS/D@Z and CuS/D@Z-FA (Both with Cy5 loaded) through intravenous injection. Mice were anesthetized with isoflurane and imaged with an IVIS system with excitation and emission wavelengths of 640 and 680 nm, respectively. At 1, 3, 6, 24 h post-injection, mice were euthanized and tumours and normal organs were immediately collected and imaged.

In vivo tumor therapy

When the tumor sizes reached ~50 mm^3, the mice were randomly divided into five groups for the treatment with PBS, CuS@Z-FA (with/without NIR irradiation) and CuS/D@Z-FA (with/without NIR irradiation). Mice were intravenously injected with different samples every other day for three times. Then tumor volume and body weight were recorded every other day. The tumor volume was calculated using the following equation: tumor volume = length × $width^2/2$. At the end of the experiment, tumors of mice in contrast treatment groups were fixed and sectioned for H&E.

Blood biochemistry

Blood and serum were obtained at day 16 after different treatments. The serum liver enzymes were tested using automatic biochemical analyzer (Hitachi-7100, Japan).

Histological examination

Isolated xenografted organs (hearts, spleens, lungs, livers, and kidneys) and tumors were fixed with 4% paraformaldehyde for 24 h. Afterwards, samples were embedded in paraffin. Paraffin sections (5 μm) were stained with hematoxylin and eosin. The specimens were analyzed blindly by a pathologist under a light microscope.

Conflicts of interest

There are no conflicts to declare.

Acknowledgements

This work was supported by Beijing Municipal Natural Science Foundation (No. 7214300), Natural Science Foundation of China (No. 82001946, 62175266), and National Key R&D Program of China (No. 2017YFB0405402).

Notes and references

1 Z. Gu, Y. Dong, S. Xu, L. Wang and Z. Liu, *Angew. Chem., Int. Ed.*, 2021, **60**, 2663.
2 X. Fu, T. Chen, Y. Song, C. Feng, H. Chen, Q. Zhang, G. Chen and X. Zhu, *Small*, 2021, **17**, 2101224.

3 H. Zhang, Z. Gao, X. Li, L. Li, S. Ye and B. Tang, *Chem. Sci.*, 2021, **12**, 12429.
4 L. Yang, H. Sun, Y. Liu, W. Hou, Y. Yang, R. Cai, C. Cui, P. Zhang, X. Pan, X. Li, L. Li, B. S. Sumerlin and W. Tan, *Angew. Chem., Int. Ed.*, 2018, **57**, 17048.
5 B. Liu, C. Li, Z. Cheng, Z. Hou, S. Huang and J. Lin, *Biomater. Sci.*, 2016, **4**, 890.
6 T. Kim, K. Nam, Y. M. Kim, K. Yang and Y. H. Roh, *ACS Nano*, 2021, **15**, 1942.
7 H. Chen, Y. Jin, J. Wang, Y. Wang, W. Jiang, H. Dai, S. Pang, L. Lei, J. Ji and B. Wang, *Nanoscale*, 2018, **10**, 20946.
8 Y. Wang, S. Li, X. Wang, Q. Chen, Z. He, C. Luo and J. Sun, *Biomaterials*, 2021, **271**, 120737.
9 M. De Palma and D. Hanahan, *Mol. Oncol.*, 2012, **6**, 111.
10 S. Y. Li, L. H. Liu, L. Rong, W. X. Qiu, H. Z. Jia, B. Li, F. Li and X. Z. Zhang, *Adv. Funct. Mater.*, 2015, **25**, 7317.
11 Y. Wan, G. Lu, J. Zhang, Z. Wang, X. Li, R. Chen, X. Cui, Z. Huang, Y. Xiao, J. Chelora, W. Zhang, Y. Liu, M. Li, H. Xie and C. Lee, *Adv. Funct. Mater.*, 2019, **29**, 1903436.
12 Z. Zhao, X. Wang, Z. Zhang, H. Zhang, H. Liu, X. Zhu, H. Li, X. Chi, Z. Yin and J. Gao, *ACS Nano*, 2015, **9**, 2749.
13 A. A. Kajani and M. A. Mehrgardi, *Nanomedicine*, 2021, **16**, 627.
14 F. Hu, B. Liu, H. Chu, C. Liu, Z. Li, D. Chen and L. Li, *Nanoscale*, 2019, **11**, 9201.
15 W. Cui, X. Lu, K. Cui, J. Wu, Y. Wei and Q. Lu, *Langmuir*, 2011, **27**, 8384.
16 L. Qiu, T. Zhang, J. Jiang, C. Wu, G. Zhu, M. You, X. Chen, L. Zhang, C. Cui, R. Yu and W. Tan, *J. Am. Chem. Soc.*, 2014, **136**, 13090.
17 S. Barman, S. K. Mukhopadhyay, S. Biswas, S. Nandi, M. Gangopadhyay, S. Dey, A. Anoop and N. D. Pradeep Singh, *Angew. Chem., Int. Ed.*, 2016, **55**, 4194.
18 J. Tang, B. Kong, H. Wu, M. Xu, Y. Wang, Y. Wang, D. Zhao and G. Zheng, *Adv. Mater.*, 2013, **25**, 6569.
19 Y. Min, J. Li, F. Liu, E. K. L. Yeow and B. Xing, *Angew. Chem., Int. Ed.*, 2014, **53**, 1012.
20 X. Meng, K. Zhang, F. Yang, W. Dai, H. Lu, H. Dong and X. Zhang, *Anal. Chem.*, 2020, **92**, 8333.
21 Z. Xie, X. Cai, C. Sun, S. Liang, S. Shao, S. Huang, Z. Cheng, M. Pang, B. Xing, A. A. A. Kheraif and J. Lin, *Chem. Mater.*, 2019, **31**, 483.
22 H. Zheng, Y. Zhang, L. Liu, W. Wan, P. Guo, A. M. Nyström and X. Zou, *J. Am. Chem. Soc.*, 2016, **138**, 962.
23 Y. Kang, X. Yu, X. Fan, Aodenggerile, S. Zhao, C. Tu, Z. Yan, R. Wang, W. Li and H. Qiu, *ACS Nano*, 2020, **14**, 4336.
24 Y. Shao, B. Liu, Z. Di, G. Zhang, L. D. Sun, L. Li and C. H. Yan, *J. Am. Chem. Soc.*, 2020, **142**, 3939.
25 O. Kwon, J. Y. Kim, S. Park, J. H. Lee, J. Ha, H. Park, H. R. Moon and J. Kim, *Nat. Commun.*, 2019, **10**, 3620.
26 T. Wen, G. Quan, B. Niu, Y. Zhou, Y. Zhao, C. Lu, X. Pan and C. Wu, *Small*, 2021, **17**, 2005064.
27 K. Ikigaki, K. Okada, Y. Tokudome, T. Toyao, P. Falcaro, C. J. Doonan and M. Takahashi, *Angew. Chem., Int. Ed.*, 2019, **58**, 6886.
28 C. Liu, Q. Sun, L. Lin, J. Wang, C. Zhang, C. Xia, T. Bao, J. Wan, R. Huang, J. Zou and C. Yu, *Nat. Commun.*, 2020, **11**, 4971.
29 B. Liu, F. Hu, J. Zhang, C. Wang and L. Li, *Angew. Chem., Int. Ed.*, 2019, **58**, 8804.
30 X. Chen, Z. Shi, R. Tong, S. Ding, X. Wang, J. Wu, Q. Lei and W. Fang, *ACS Biomater. Sci. Eng.*, 2018, **4**, 4183.
31 H. Zhang, W. Jiang, R. Liu, J. Zhang, D. Zhang, Z. Li and Y. Luan, *ACS Appl. Mater. Interfaces*, 2017, **9**, 19687.
32 Q. L. Li, Y. Sun, L. Ren, X. Wang, C. Wang, L. Li, Y. W. Yang, X. Yu and J. Yu, *ACS Appl. Mater. Interfaces*, 2018, **10**, 29314.